Phys. Lett. B 862 (2025) 139324

Contents lists available at ScienceDirect

Physics Letters B

journal homepage: www.elsevier.com/locate/physletb

Letter

Emergence of magnetic dipole band in ^{88}Sr due to novel stretched coupling scheme

B. Das [a,b,*], Md.S.R. Laskar [a,c], R. Palit [a,*], S. Rajbanshi [d], V. Malik [a], F.S. Babra [a], S. Chattopadhyay [e], Biswajit Das [a], P. Dey [a], A. Kundu [a]

[a] Department of Nuclear and Atomic Physics, Tata Institute of Fundamental Research, Mumbai 400005, India
[b] GSI Helmholtzzentrum für Schwerionenforschung GmbH, Darmstadt, Germany
[c] Istituto Nazionale di Fisica Nucleare (INFN), Sezione di Milano, Milan 20133, Italy
[d] Department of Physics, Presidency University, Kolkata 700073, India
[e] Saha institute of nuclear physics, 1/AF, Bidhannagar, Kolkata 700064, India

ARTICLE INFO

Editor: B. Blank

ABSTRACT

High spin states of ^{88}Sr have been populated using ^{13}C + ^{82}Se reaction. The structure of a negative parity band consisting of six magnetic dipole transitions with energies of 605 - 490 - 311 - 267 - 528 - 974 keV extending up to $I^{\pi} = 13^{-}$ was investigated through lifetimes measurements using Doppler Shift Attenuation Method (DSAM). The extracted transition strengths from the measured lifetimes initially increase with spin and then decrease beyond $I^{\pi} = 10^{-}$. The observed gamma-ray energy behaviour and that of transition rates were explained using a novel stretched coupling scheme. In this geometrical model, an interplay between a particle-particle attractive shears and two particle-hole repulsive shears has been invoked to explain the observed behaviour. This confirms the existence of an attractive shears between two particle blades for the first time in any nuclei.

1. Introduction

The complex gyroscopic motions of the nucleons near the Fermi surface and their coupling continue to surprise us with new emergent properties of nuclei at high spin. The gyroscopic behaviour was first seen in deformed nuclei, where a correlated motion of all the nucleons generate the high spin states under the adiabatic approximation [1]. On the other hand, the angular momentum stretched coupling scheme, proposed by Danos and Gillet [2] describes the excited states in deformed nuclei using the shell model basis states of nucleons outside the core, and provided important insight in to the high spin generation mechanism in nuclei. Recently, the rotation in nuclei along the N = Z line was explained using the mutual alignment of stretched angular momentum blades formed by protons and neutrons residing in the same quantum orbitals. The spin aligned isoscalar paired phase found in ^{92}Pd [3] and ^{88}Ru [4] nuclei supports this conjecture. A further implication of stretched coupling scheme was found in terms of shears mechanism, to explain the rotation like band formation in near spherical Pb nuclei [5–8]. The concept of the shears bands was first reported in Ref. [9] to explain the results of the self-consistent tilted axis cranking calculation. The predicted large $B(M1, I \rightarrow I-1)$ values and their decrease with I, the hallmarks of magnetic rotation, were later confirmed in Ref. [10]. The intriguing phenomena of shears mechanism introduced a new kind of rotational symmetry, and was extended further to explain multitude of phenomena in the nuclear landscape [11].

The concept was further generalized using a simple phenomenological approach, where most of the features of tilted axis cranking model could be explained by assuming an effective potential of the form $V_2 P_2(\theta)$ as a function of shears angle, θ [12], where V_2 is the strength of the effective interaction between two shears blades. For a particle-hole shears, a positive sign of V_2 reflects the repulsive nature of the interaction. On the other hand, a negative sign of V_2 accounts for the particle-particle and hole-hole shears, as predicted by Macchiavelli et al., [12]. However, all the studied magnetic rotational bands were found to be of the former character, backed by the observation of the signature trend of increasing M1 energies and falling B(M1) rates with increasing spin [10]. The examples corresponding to shears bands in which the blades are both made from particles or both made from holes of shears bands have been predicted to exist in nuclei, however, no clear sign of increasing $M1$ energy accompanied by increasing transition rates strength

* Corresponding authors.
E-mail addresses: b.das@gsi.de (B. Das), palit@tifr.res.in (R. Palit).

https://doi.org/10.1016/j.physletb.2025.139324
Received 4 July 2024; Received in revised form 29 December 2024; Accepted 13 February 2025

Available online 14 February 2025

values has been reported yet. It is worthwhile to mention here that, the attractive shears term was included previously to explain the behaviour of rotational bands [13,14], however, the signature trend was missing due to the interplay with other modes of excitation. In this sense, for the first time a clear signature trend of energy and transition rates in ^{88}Sr makes the proof of attractive shears mechanism conclusive.

Apart from the Pb region, the nuclei in the A$\sim$ 110 region [10] were proved to be a versatile testing ground for various modes of shears mechanism. With protons residing in the $40 < Z < 50$ shell orbitals, and neutrons lying above the $N = 50$ shell gap, the proton and neutron Fermi levels in these nuclei provided the essential particle-hole structures to observe the shears mechanism in play upon excitation [14–22]. In particular, these quantum states become available for ^{88}Sr, once the protons are promoted above the $Z = 40$ semi-shell closure along with an excited neutron core. In the previous studies by Stefanove et al., [23,24] a negative parity high-spin band was established with tentative bandhead at $I^{\pi} = 7^{-}$. This band shows the decreasing M1 energies with increasing spin until $I^{\pi} = 11^{-}$, a signature trend for attractive shears. Moreover, Stefanova et al., predicted the quasiparticle configuration $\pi[1p_{3/2}^{-1}0g_{9/2}] \otimes \nu[0g_{9/2}^{-1}1d_{5/2}]$ for the $I^{\pi} = 8^{-}$ state [23]. This configuration is suitable to form a particle-particle shears if stretchly coupled. However, the lifetime of the levels were not measured to establish the nature of transition rates under shears mechanism.

In this work, the high spin states of ^{88}Sr were studied. We have established the negative parity band structure firmly, by measuring the spin and parity of the levels within the band. The mean lifetimes were measured for the negative parity states using Doppler Shift Attenuation Method (DSAM). The observed energy behaviour and that of transition rates were explained using the geometrical model of shears mechanism. An interplay between a particle-particle attractive shears and two particle-hole repulsive shears were necessary to explain the observed behaviour. This confirms the existence of an attractive shears between two particle blades for the first time in any nuclei. It is here to be noted here that, attractive shears mechanism has been taken into account in explaining the energy systematic in ^{144}Dy [13]. However, without the transition rate values, the claim is inconclusive.

2. Experimental details and data analysis

The high spin states of ^{88}Sr were populated by bombarding ^{13}C nuclei at 60 MeV on a 1 mg/cm^2 thick ^{82}Se target. The ^{13}C beam was provided by the Pelletron-Linac facility at the Tata Institute of Fundamental Research (TIFR), Mumbai. The target was backed with a 4.26 mg/cm^2 thick ^{197}Au foil to stop the recoiling nuclei. γ-rays from the de-exciting nuclei were detected using 11 Compton suppressed Clover detectors of Indian National Gamma Array (INGA), TIFR [25]. The level scheme of ^{88}Sr was analysed from 2-fold coincidence data. Although no new transition was observed, we confirm the existing level-scheme established by Stefanova et al. [23]. The spin and parities of the energy levels were confirmed using the DCO [26] and iPDCO ratios [27]. The measured γ-ray energies, intensities, DCO and iPDCO ratios for the partial level scheme are tabulated in Table 1. Details of the experimental setup could be found in Ref. [28]. The sub-picosecond mean level lifetimes were measured for the negative parity band using DSAM. The LINESHAPE code by Wells and Johnson [29] was used to generate the velocity profile of nuclei recoiling into the backing. The velocity profile contained 10000 histories with a time step of 0.001 ps. The lineshapes were calculated for the 90^0, 140^0 and 157^0 detector angles with respect to the beam direction. Although the spectrum at 90^0 angle shows no lineshape, it was included in to the fit to identify any contaminants altering lineshapes at other angles. The Doppler broadening at 90^0 was also taken care of by the LINESHAPE code using the detector geometry information. For energy loss calculation, the Northcliff and Shilling shell correction method [30] was used. The line shapes were simulated on the co-incidence spectra from the angle dependent asymmetric matrices where the co-incidence was taken with transitions both residing bottom as well as top of the level. For the negative parity band, the 974.2 keV ($13^{-} \rightarrow 12^{-}$) transition lineshape was fitted assuming a 100% side feed. This gives an effective lifetime for the 13^{-} level. Lower lying transitions were then fitted into a cascade to evaluate the mean level lifetimes using the 605.4($8^{-} \rightarrow 7^{-}$) keV gate (Fig. 1(a)). The 605.4($8^{-} \rightarrow 7^{-}$) keV transition lineshape was extracted (Fig. 1(b)) using the top gate, where the fitting involves a four level cascade with the 11^{-} level's lifetime as effective. The measured lifetimes are tabulated in the Table 2. It is to be noted here that, the mean life for the 12^{-} state was previously measured by Stefanova et al., to be $\tau(12^{+}) = 0.8(3)$ ps, while our measurement gives a significant different value of $\tau(12^{+}) = 0.23(10)$ ps.

Table 1
The energy, intensity, DCO and iPDCO values of the γ-rays belonging to the ^{88}Sr nucleus.

$I_i^{\pi_i} \rightarrow I_f^{\pi_f}$	Energy(keV)	Intensity	DCO	iPDCO
$13^{+} \rightarrow 12^{+}$	180.9	7.6(1)	0.76(04)[2]	
$12^{+} \rightarrow 12^{+}$	241.0	7.9(1)	2.08(01)[2]	
$11^{-} \rightarrow 10^{-}$	266.8	13.6(2)	0.37(01)[1]	
$8^{-} \rightarrow 7^{+}$	267.0	4.0(2)		
$10^{-} \rightarrow 9^{-}$	311.3	9.9(2)	0.32(01)[1]	
$7^{-} \rightarrow 7^{-}$	319.9	3.6(2)		
$12^{+} \rightarrow 11^{+}$	319.4	19.2(3)	0.30(02)[1]	-0.14(02)
$11^{+} \rightarrow 10^{+}$	340.4	8.0(2)	0.25(02)[1]	-0.09(01)
$7^{-} \rightarrow 6^{-}$	348.0	48.2(4)	0.32(01)[1]	-0.17(01)
$6^{-} \rightarrow 5^{-}$	434.4	71.1(5)	0.85(01)[1]	-0.21(01)
$15^{+} \rightarrow 14^{+}$	449.4	9.6(1.0)	0.33(02)[1]	-0.10(02)
$9^{-} \rightarrow 8^{-}$	490.2	14.6(2)	0.24(01)[1]	-0.00(01)
$12^{-} \rightarrow 11^{-}$	528.5	8.1(3)	0.32(01)[1]	-0.00(01)
$10^{-} \rightarrow 10^{+}$	523.3	1.8(1)		
$12^{+} \rightarrow 11^{+}$	561.1	4.7(1)	0.90(01)[2]	
$13^{+} \rightarrow 12^{+}$	561.0	1.0(5)		
$7^{+} \rightarrow 6^{+}$	581.8	1.8(1)		
$14^{+} \rightarrow 13^{+}$	592.2	15.4(10)		-0.10(01)
$13^{+} \rightarrow 12^{+}$	599.5	12.4(9)		-0.09(01)
$8^{-} \rightarrow 7^{-}$	605.4	12.3(4)	0.35(02)	
$17^{+} \rightarrow 16^{+}$	616.5	8.0(10)	0.37(05)[1]	-0.04(01)
$11^{+} \rightarrow 10^{+}$	655.2	9.2(1)		
$13^{+} \rightarrow 13^{+}$	659.6	6.1(1)		
$16^{+} \rightarrow 15^{+}$	761.4	8.7(10)	0.27(02)[1]	-0.08(02)
$7^{-} \rightarrow 5^{-}$	783.0	7.4(1)	0.91(09)[1]	
$13^{+} \rightarrow 12^{+}$	841.1	3.8(1)	0.96(02)[2]	-0.13(05)
$5^{-} \rightarrow 3^{-}$	850.2	90.9(5)	0.81(02)[1]	0.05(01)
$6^{+} \rightarrow 5^{-}$	936.1	8.9(3)		
$13^{-} \rightarrow 12^{-}$	974.2	2.9(3)		
$7^{+} \rightarrow 6^{-}$	1083.4	8.7(2)	0.34(03)[1]	-0.11(01)
$7^{-} \rightarrow 7^{+}$	1132.0	5.6(4)		
$8^{+} \rightarrow 7^{-}$	1287.1	34.9(2)	0.53(02)[1]	
$10^{+} \rightarrow 8^{+}$	1464.0	18.6(6)	1.91(06)[2]	
$8^{-} \rightarrow 7, 8$ [4]	1469.7	2.2(1)		
$7^{-} \rightarrow 6^{+}$	1714.2	5.8(2)		
$10^{+} \rightarrow 8^{+}$	1779.1	12.7(2)	2.06(11)[2]	0.08(01)
$2^{+} \rightarrow 0^{+}$	1836.2	100.0(1)[3]		
$7^{-} \rightarrow 7^{-}$	1867.5	4.3(2)		
$9^{-} \rightarrow 8^{+}$	1903.7	3.4(1)		
$8^{-} \rightarrow 7^{-}$	2154.4	3.5(1)		

[1] Gating transition is of stretched multipolarity $\Delta I = 2$.
[2] Gating transition is of stretched multipolarity $\Delta I = 1$.
[3] Itensities are normalised with respect to this transition.
[4] Tentative spin of final state is adopted from Ref. [23].

3. Discussion

The deduced M1 transition rates show a steep increase from $I^{\pi} = 7^{-} \rightarrow 10^{-}$, and can be ascribed to the signature of an attractive shears mechanism in play. On the other hand, the B(M1) rates start falling beyond $I^{\pi} = 11^{-}$. To account for this phenomena we can construct a stretchly coupled angular momentum scheme using the quasiparticle configuration $\pi[1p_{3/2}^{-1}0g_{9/2}] \otimes \nu[0g_{9/2}^{-1}1d_{5/2}]$, shown in Fig. 2.(a). In this scheme, the particle blades are composed of a $0g_{9/2}$ proton (j_{p1}) and a $1d_{5/2}$ neutron (j_{p2}), which align anti-parallely at the bandhead to open up an attractive shears. The $\pi(1p_{3/2}^{-1})$ and $\nu(0g_{9/2}^{-1})$ holes on the other

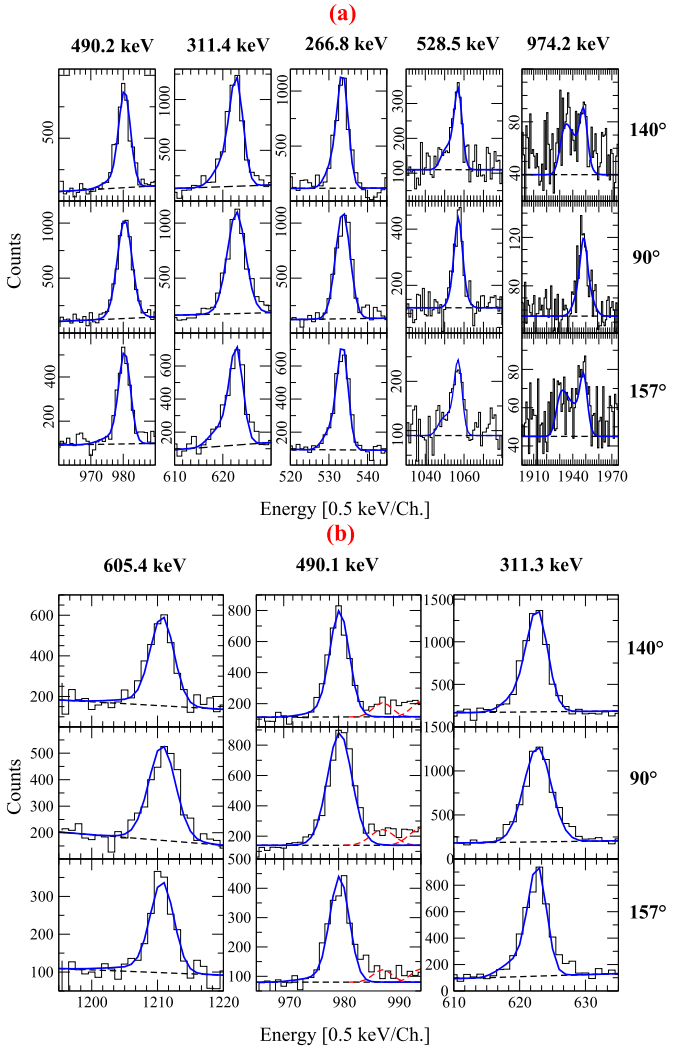

Fig. 1. (a) Lineshapes of the γ transitions decaying from the high spin negative parity states of ^{88}Sr. The lineshapes were extracted using the (a) 605.5($8^- \rightarrow 7^-$) keV gate and (b) the 528.5($12^- \rightarrow 11^-$) keV top gate.

Table 2
Experimental lifetimes and B(M1) strengths for the negative parity band of ^{88}Sr. The theoretical B(M1) values are calculated using the g-factor(orbital) values +1.40 ($\pi g_{9/2}$), -0.52($\nu d_{5/2}$) for the first set and an effective g-factor value of g_{eff} (g_{p1} - g_{p2}) = 3.2 for the second set using Eq. (6).

$I_i^\pi \rightarrow I_f^\pi$	τ	B_{EX}(M1)	B(M1) g_{p1} = 1.40, g_{p2} = -0.52	B(M1) g_{eff} = 3.2
	[ps]	[μ_N^2]	[μ_N^2]	[μ_N^2]
$7^- \rightarrow 6^-$			0.47	1.29
$8^- \rightarrow 7^-$	0.35(12)	$0.73^{+0.38}_{-0.19}$	1.11	3.09
$9^- \rightarrow 8^-$	0.28(10)	$1.72^{+0.96}_{-0.45}$	1.72	4.79
$10^- \rightarrow 9^-$	0.27(10)	$6.94^{+4.08}_{-1.87}$	2.13	5.91
$11^- \rightarrow 10^-$	0.45(12)	$6.55^{+2.38}_{-1.38}$	2.17	6.03
$12^- \rightarrow 11^-$	0.23(10)	$1.67^{+1.29}_{-0.51}$	1.70	4.73
$13^- \rightarrow 12^-$	0.41	0.15	0.61	1.68

hand, are aligned perpendicular to their conjugate particle blades. This configuration maximizes the wave function overlap, and hence constitute the bandhead. The spin of this stretched configuration can be constructed as

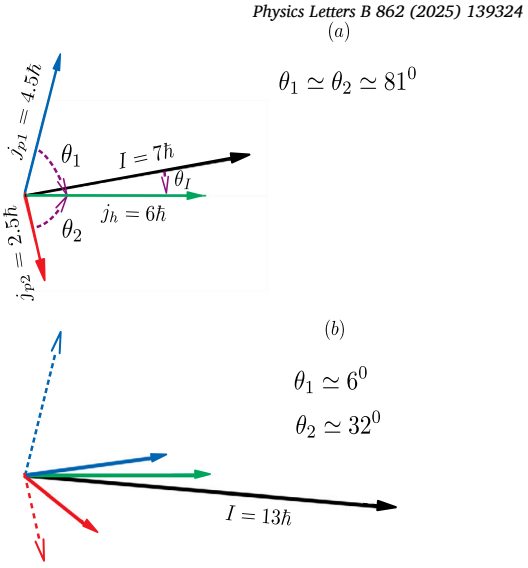

Fig. 2. The stretch coupling scheme for the negative parity band of ^{88}Sr at the (a) bandhead at $I^\pi = 7^-$ and at the (b) band termination at $I^\pi = 13^-$ using the quasiparticle configuration $\pi[1p_{3/2}^{-1}0g_{9/2}] \otimes \nu[0g_{9/2}^{-1}1d_{5/2}]$. j_{p1} and j_{p2} are the spin of the proton and neutron particles respectively, where j_h is the total spin of the aligned neutron and proton holes.

$$I^2(\theta_1,\theta_2) = j_{p1}^2 + j_{p2}^2 + j_h^2 + 2j_{p1}j_{p2}cos(\theta_1+\theta_2) + 2j_h[j_{p1}cos(\theta_1) + j_{p2}cos(\theta_2)] \quad (1)$$

where θ_1 and θ_2 are the shears angles and depicted in Fig. 2(a). With the alignment of particle blades, the energy of each state can be calculated using the geometrical model [13] as

$$E = E_0 + \frac{V_1}{2}\frac{1}{2}[3cos^2(\theta_1) - 1] + \frac{V_2}{2}\frac{1}{2}[3cos^2(\theta_2) - 1] - \frac{V_{pp}}{2}\frac{1}{2}[3cos^2(\theta_1+\theta_2) - 1] \quad (2)$$

where, E_0 is the bandhead energy, V_1 and V_2 are the effective shears potential for two repulsive shears formed by j_{p1} and j_{p2} blades respectively with their conjugate hole blades and V_{pp} is the attractive shears potential between two particle blades. The validity of this equation has been checked using the simple approximation of $V_{pp} = V_1 = V_2 = V$ [13]. This reduces the degrees of freedom to one, and the shears angles at the two extremes of the alignment were found using the energy minimization condition

$$\frac{dE}{d\theta} = 0 \quad (3)$$

where, $\theta_1 = \theta_2 = \theta$. An analytical solution gives, $\theta_{max} = 90°$ and $\theta_{min} = 30°$, which can be fed back in to Eq. (1) to get the band spins at two extremes as follows

$$I(\theta_{max}) = 6.78 \simeq 7$$
$$I(\theta_{min}) = 13.40 \simeq 13 \quad (4)$$

This validates the shears model as a plausible mode to describe the angular momentum generation mechanism for the negative parity band of ^{88}Sr. However, to calculate the proper transition rates, the non equality of shears potentials needs to be taken into consideration.

A relation can be established between V_1 and V_2 using the relative amplitudes of j_1 and j_2, which is [14],

$$\theta_2 = \theta_2^i(\theta_1/\theta_1^i)^\alpha \quad (5)$$

where, the scaling factor, $\alpha = (j_{p1} - j_{p2})/j_{p1}$, taken empirically to adjust the relative shears closing speed for the particle blades with respect to their conjugate hole blades. The shears angles obtained using Eq. (5)

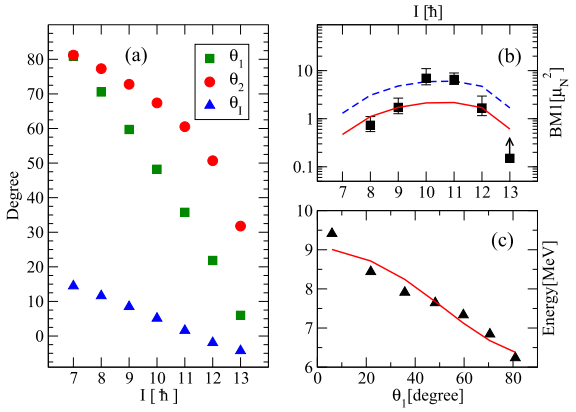

Fig. 3. (a) Angles between the shears blades as a function of spin (b) the B(M1) values as a function of spin and the (c) level energies as a function of shears angle (θ_1), for the negative parity band of ^{88}Sr nucleus. The theoretical B(M1) values are depicted as solid (dashed) line using the standard (effective) g-factor values using Eq. (6).

and Eq. (1), are plotted in Fig. 3(a). The obtained shears angles were used to calculate the B(M1) rates using the relation [31]

$$B(M1) = \frac{3}{4\pi}(g_{p1} - g_{p2})^2 \frac{(2j_{p1}+1)^2(2j_{p2}+1)^2}{16I(I+1)} sin^2(\theta_1 + \theta_2) \quad (6)$$

where, g_{p1} and g_{p2} are the g-factors for proton and neutron blades respectively. As depicted in Fig. 3(b), the calculated B(M1) values reproduces the trend pretty well. However, the amplitude deviates more in the mid spin region and can be reproduced using an effective gyromagnetic ratio, $g_{eff} = 3.2$. A plausible explanation for this deviation could be the reopening of the hole blades with increasing spin, due to the non-equality of V_1 and V_2, and this was neglected in our calculation. Finally, the energy of the band was fitted using Eq. (2) to obtain the shears potentials. A reasonable fit to the level energies, depicted in Fig. 3(c), was obtained using shears potentials $V_1 \simeq 1.8$ MeV, $V_2 \simeq 2.2$ MeV and $V_{pp} \simeq 1.8$ MeV.

4. Summary

In conclusion, by studying the high-spin states of ^{88}Sr, we could assign the configuration $\pi[1p_{3/2}^{-1}0g_{9/2}] \otimes \nu[0g_{9/2}^{-1}1d_{5/2}]$ at the band head for the negative parity band, under the assumption of stretched coupling scheme. This coupling allows for a particle-particle shears to be formed and the shears closing was attributed solely for the formation of band structure. The assignment is also supported by the fact that the negative parity band is exhausted at $I^\pi = 13^-$, the maximally aligned state. The energy and transition rates systematic was explained using the competition between an attractive and two repulsive shears between the stretchly coupled angular momentum blades. Thus, in the negative parity band of ^{88}Sr, for the first time an attractive shears mechanism was seen to be taking part in generating the high spin states. It is important to mention here that, the proton excitation across the $Z = 40$ semi-shell gap coupled with the neutron core excitation [23] makes this stretch configuration possible so that particle blades of opposite characters could be formed. One could expect to find more attractive shears bands in nuclei with similar quasi-particle configurations.

Declaration of competing interest

The authors declare that they have no known competing financial interests or personal relationships that could have appeared to influence the work reported in this paper.

Acknowledgement

Authors are grateful to the staff at TIFR-BARC Pelletron Linac Facility for providing good quality beam and smooth operation of the accelerator for the entire duration of the experiment. The help and cooperation from B. S. Naidu, S. Jadhav, Abraham T. Vazhappilly and R. Donthi for setting up the experimental apparatus is acknowledged. This work is supported by the Department of Atomic Energy, Government of India (Project Identification No. RTI 4002), and the Department of Science and Technology, Government of India (Grant No. IR/S2/PF-03/2003-II).

Data availability

Data will be made available on request.

References

[1] A. Bohr, A. Mottelson, Nuclear Structure, vol. 2, Benjamin, New York, 1974.
[2] Micheal Danos, Vincent Gillet, Phys. Rev. 161 (1967) 160.
[3] B. Cederwall, et al., Nature (London) 469 (2011) 68.
[4] B. Cederwall, et al., Phys. Rev. Lett. 124 (2020) 062501.
[5] R.M. Clark, et al., Phys. Lett. B 275 (1992) 247;
G. Baldsteifen, et al., Phys. Lett. B 275 (1992) 252;
A. Kuhnert, et al., Phys. Rev. C 46 (1992) 133.
[6] R.M. Clark, et al., Phys. Lett. B 440 (1998) 251–256.
[7] H. Hübel, Prog. Part. Nucl. Phys. 54 (2005) 1–69.
[8] R.M. Clark, A.O. Macchiavelli, Annu. Rev. Nucl. Part. Sci. 50 (2000) 1.
[9] S. Frauendorf, Nucl. Phys. A 557 (1993) 259c.
[10] R.M. Clark, et al., Phys. Rev. Lett. 82 (1999) 3220.
[11] S. Frauendorf, Rev. Mod. Phys. 73 (2001) 463.
[12] A.O. Macchiavelli, et al., Phys. Rev. C (R) 57 (1998) 3.
[13] M. Sugarwara, et al., Phys. Rev. C 79 (2009) 064321.
[14] E.O. Podsvirova, et al., Eur. Phys. J. A 21 (2004) 1.
[15] P. Datta, et al., Phys. Rev. C 71 (2005) 041305.
[16] P. Datta, et al., Phys. Rev. C 78 (2008) 021306(R).
[17] S. Roy, S. Chattopadhyay, Phys. Rev. C 83 (2011) 024305.
[18] S. Roy, et al., Phys. Lett. B 694 (2011) 322–326.
[19] S. Rajbanshi, et al., Phys. Rev. C 89 (2014) 014315.
[20] B. Das, et al., Phys. Rev. C 93 (2016) 064322.
[21] B. Das, et al., Phys. Rev. C 95 (2017) 051301(R).
[22] B. Das, et al., Phys. Rev. C 98 (2018) 014326.
[23] E.A. Stefanova, et al., Phys. Rev. C 62 (2000) 054314.
[24] E.A. Stefanova, et al., Nucl. Phys. A 669 (2000) 14–26.
[25] R. Palit, et al., Nucl. Instrum. Methods Phys. Res., Sect. A 622 (2010) 281.
[26] A. Krämer-Flecken, et al., Nucl. Instrum. Methods Phys. Res., Sect. A 275 (1989) 333.
[27] K. Starosta, et al., Nucl. Instrum. Methods Phys. Res., Sect. A 113 (2012) 1315.
[28] S. Saha, et al., Phys. Rev. C 99 (2019) 054301.
[29] J.C. Wells, N.R. Johnson, LINESHAPE: a Computer Program for Doppler-Broadened Lineshape Analysis, Report No. ORNL-6689, 1991.
[30] L.C. Northcliffe, R.F. Schilling, Nucl. Data Tables 7 (1970) 233.
[31] P. Van Isacker, A.O. Macchiavelli, Phys. Rev. C 87 (2013) 061301(R).